Crystal Structures of *n*-Alkane with Three Functional Groups in the Middle and at Both Ends

Hiroko Yamamoto,* Satoshi Teshima,† and Norio Nemoto‡

Department of Molecular and Material Sciences, IGSES, Kyushu University, 6-1 Kasuga-koen, Kasuga, Fukuoka 816-8580, Japan

Kohji Tashiro

Department of Future Industry-Oriented Basic Science and Materials, Toyota Technological Institute, 2-12-1 Hisakata, Tempaku, Nagoya 468-8511, Japan

Received: September 14, 2008; Revised Manuscript Received: November 15, 2008

We synthesized a linear alkane, K35DA, with a main-chain carbon number $n = 33$ and three functional groups, a carbonyl group in the middle and carboxyl groups at both ends, and studied influences of the functional groups as well as chain length on morphologies of samples prepared by solution-grown and bulk crystallization methods (SG-K35DA and BK-K35DA) from differential scanning calorimetry (DSC), X-ray diffraction, and IR absorption measurements. Data analyses reveal that at room temperature an orthorhombic crystal of type $P2_12_12_1$, together with a considerable amount of amorphous fraction, is predominantly realized in BK-K35DA due to the van der Waals force between neighboring long methylene sequences, whereas a monoclinic type of crystal belonging to the same space group ($P2_1/c$) as reported for linear dicarboxylic acid crystals with odd carbon numbers is coexistent for SG-K35DA. The crystalline structures appear to be distorted with increasing temperature, as the dipole−dipole interaction between the carbonyl groups tends to be weakened, and both orthorhombic and monoclinic crystals undergo the solid−solid phase transition to the hexagonal crystalline structure at a temperature about 10 K below their respective T_ms, which can be regarded as a new example of the Brill transition.

Introduction

Attachment of carboxylic acids to both ends of linear alkane molecules gives rise to cyclic dimers between two carboxylic acids due to hydrogen bonding, which leads to very long chains.[1,2]Their backbone chain conformations and the electrostatic repulsive forces between oxygen atoms of neighboring dimers, together with the van der Waals interaction between long methylene chains, play a deterministic role for chain packing in crystal formation.[3−10] Constructing a geometrical model based on the above factors, Boese and collaborators[11−14] successfully interpreted the phenomenon of melting point alteration known for short-chain *n*-alkanes as well as α,ω-disubstituted *n*-alkane derivatives. This model could very closely predict crystal structures of α,ω-alkanedicarboxylic acids with carbon number $n \geq 5$ experimentally found in such a way that (1) diacids with an even number of carbons *n* take a monoclinic form (space group $P2_1/c$) with orthorhombic subcell; (2) diacids with odd *n* exhibit dimorphism composed of two monoclinic forms, α (space group $P2_1/c$) and β (space group $C2/c$), neither of whose subcells are orthorhombic.[1−11] Linear alkanes with even *n* are known to take the monoclinic form for $n \geq 26$ with the same orthorhombic subcell as those with odd *n*, which is the real subcell for polyethylene.[15−20] We may consider that the subcell structure where the backbone carbon plane is vertical to the corresponding plane of the closest neighboring chain to each other is the most stable chain packing form for hydrophobic methylene chains of sufficiently large *n*. According to the geometrical model, the trans zigzag type of conformation corresponding to the above chain packing is naturally realized for diacids with even *n*, whereas methylene chains of diacids with odd *n* must take a twisted molecular conformation with severe torsions in order to reduce the repulsive force between the cyclic dimers. Competition between this conformation with high energy and the all-trans conformation with the lowest energy would become severe with increasing main-chain length, and it might result that diacids with odd *n* could take chain packing so as to form the orthorhombic subcell for sufficiently large *n*.

Carbonyl groups in symmetrical ketone crystals are regularly aligned on the plane vertical to the long *n*-alkane main chain so that strong dipole−dipole interaction between two planes apart by one molecular chain length prohibits solid−solid phase transitions characteristic of the corresponding *n*-alkane chains and raises its melting temperature T_m considerably.[15−28] Because of the carbonyl group's small size, however, the symmetrical ketone keeps the same crystal structure as its linear homologue. Therefore, introduction of the carbonyl group into the middle of the main chain of diacids may not perturb the crystal structure but stabilize it against thermal agitation, inducing local molecular motion, up to higher temperature.

In a series of papers,[29−34] Tashiro and collaborators studied the Brill transition using well-characterized aliphatic nylon samples as well as model low molecular weight compounds. Analyses of X-ray diffraction data and infrared progression bands have revealed that the concept of the order−disorder

* To whom correspondence should be addressed: tel +8192-583-8820; e-mail yamamoto@mm.kyushu-u.ac.jp.

† Present address: Mitsubishi Plastics Inc., 5-8 Mitsuya, Nagahama, Shiga 526-8660, Japan.

‡ Present address: 894-550 Yufuin, Yufu, Oita 879-5114, Japan.

10.1021/jp808176n CCC: $40.75
Published on Web 02/16/2009

SCHEME 1

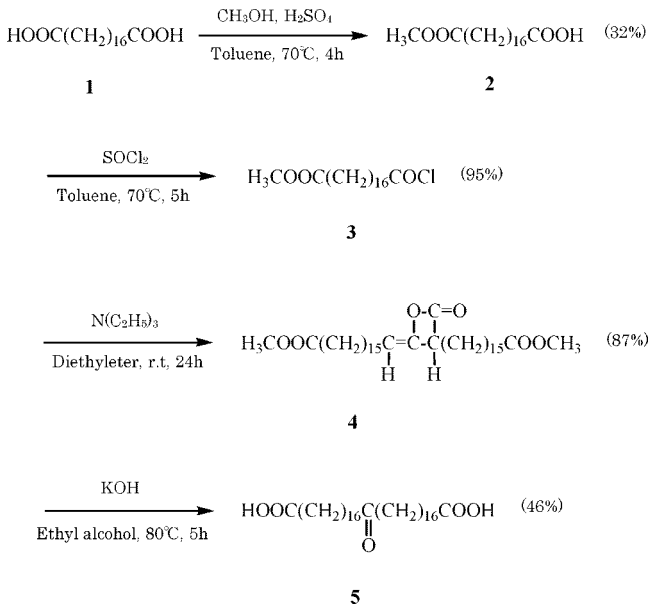

transition is more reasonably applicable for the phase transition behaviors of all the samples tested, while the Brill transition was originally proposed as the solid−solid phase transition phenomenon, even though it gradually proceeds with a rise in temperature.[35−44] The model compounds used by them are packed together with intermolecular hydrogen bonds between the neighboring amide groups to form a sheetlike structure and are stacked by the weak van der Waals force along the main-chain direction. α,ω-Alkanedicarboxylic acids with the carbonyl group in the middle can be regarded as thermoreversible polymers and are tightly packed by the dipole−dipole interaction between the carbonyl groups aligned in the plane. Thus it seems worthwhile to examine whether this low molecular weight substance exhibits phase transition behaviors close to the Brill transition with increasing temperature.

In this paper, we synthesized a linear alkane, K35DA, with a main-chain carbon number $n = 33$ with three functional groups, a carbonyl group in the middle and carboxyl groups at both ends, and performed differential scanning calorimetry (DSC), X-ray diffraction, and IR absorption measurements on samples prepared by the solution-grown and the bulk crystallization methods over a wide temperature range. We found that K35DA samples exhibit quite complicated morphologies affected by an increase in the main chain length at room temperature and undergo the solid−solid phase transition at elevated temperature characteristic of the Brill transition.

Experimental Section

Materials. The long-chain *n*-alkane with main-chain carbon number $n = 33$, with a carbonyl group in the middle and carboxyl groups at both ends, 18-oxopentatriacontanedioic acid $[HOOC(CH_2)_{16}]_2C{=}O$ (denoted K35DA), was synthesized through ketene dimerization reaction using the corresponding carbonic acid chlorides free from other homologues as shown in Scheme 1. The corresponding linear *n*-alkane C35 and symmetrical ketone K35 with a carbonyl group in the middle of the main chain were also synthesized for comparison.

Carboxylic acid monoester **2** was obtained by reacting only one end of the corresponding carboxylic diacid **1** (Tokyo Kasei Co., purity; minimum 98.0%), and carboxylic acid chloride monoester **3** was synthesized by use of thionyl chloride from **2**. Product **3** was further reacted under argon atmosphere in ether solution with tertiary amine to obtain alkyl ketene dimer **4**, which was easily converted to dicarboxylic acid with the carbonyl group in the middle (**5**) by hydrolysis. K35 was also synthesized through a ketene dimerization reaction, and C35 was reduced from K35 via the Wolff−Kishner method.[45,46] Products obtained were finally purified by elution and recrystallization through a silica column with hexane and diethyl ether as solvents, respectively, and identified from IR and NMR measurements. Sample purity was determined with a capillary gas chromatograph (GC-14A, Shimadzu) equipped with a column of CBP1-M25-025. The purity for homologues was up to 99.7% for all samples. Solution-grown (SG) crystallization of C35 (SG-C35), K35 (SG-K35), and K35DA (SG-K35DA) was performed with 3% toluene solution. Bulk-crystallized K35DA (denoted BK-K35DA) was prepared with a slow cooling rate of 2.0 K h^{-1} from the melt at 420 K.

Methods. DSC measurements were performed on a calorimeter (DSC-8240B with a TAS-100 controller, Rigaku) from 273 to 423 K for all samples. The standard heating rate of 1.0 K min^{-1} was employed under dry nitrogen atmosphere for a sample mass of about 1.0 mg. The heating rate dependence was examined and found to be negligible. Temperature calibration was performed with indium (In) and also shorter *n*-alkanes with known equilibrium melting temperatures. The heat of transition or fusion was calibrated with In and gallium.

IR spectra were obtained at 11 temperatures from room temperature to T just below the respective melting temperatures of SG- and BK-K35DA, by use of a Fourier transform infrared (FT-IR) spectrometer (FTS-6000, Bio-Rad) with 32 scans at the highest resolution of 2 cm^{-1}. The samples were prepared by mixing with KBr powder and then pressing to make a disk. IR spectra were also obtained for SG-K35 at 10 temperatures from room temperature to T just above its melting temperature and for heptadecanedioic acid, C17DA, for comparison. The X-ray diffraction measurements were performed for SG samples of C35, K35, and K35DA with a diffractometer using Ni-filtered Cu Kα radiation (Geigerflex 2027, Rigaku) at room temperature and also for SG- and BK-K35DA at 10 and 12 temperatures from room temperature to T just below their melting temperatures, respectively.

Results and Discussion

Thermal Behaviors. Figure 1 shows DSC thermograms measured for SG-C35, SG-K35, SG-K35DA, and BK-K35DA. The curve for SG-C35 unambiguously exhibits the B, C, and H solid−solid phase transitions at 332, 339, and 345 K, respectively, and a sharp melting peak at 347.5 K. There is no peak corresponding to the solid−solid phase transition in the curve for SG-K35 and melting occurs at 361.6 K, considerably higher than the T_m of SG-C35, which is interpreted as being due to the dipole−dipole interaction between carbonyl groups as described in the Introduction. Thermograms for SG-K35DA and BK-K35DA samples indicate that, above about 370 K, there starts a weak endothermic process, which is smoothly followed by the melting process. The former process may be attributed to onset of molecular motions, while preserving the crystalline structure at room temperature, and might be regarded as the heat absorption process accompanied by the Brill transition. Their melting peaks are both broad as compared with peaks of SG-C35 and SG-K35, and the melting temperatures T_m are 400.7 and 395.6 K, respectively, being much higher than the T_ms of SG-C35 as well as SG-K35. A rise in T_m is caused by cyclic dimer formation between two carboxyl groups at both chain

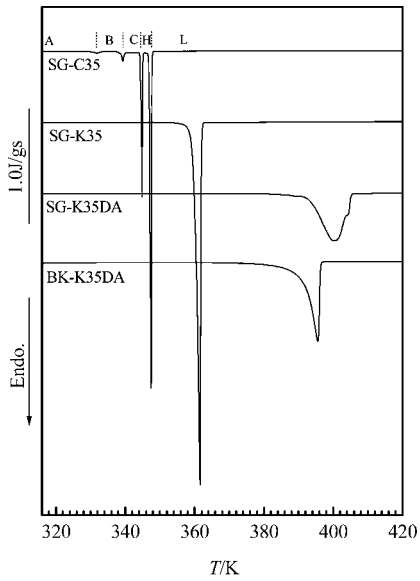

Figure 1. DSC curves of SG-C35, SG-K35, SG-K35DA, and BK-K35DA. SG-C35 exhibits solid−solid phase transitions from A, B, C, and then H phases with increasing temperature, whereas SG-K35 does not show any solid−solid phase transition due to dipole−dipole interaction between carbonyl groups. K35DA samples melt at higher temperatures because of cyclic dimer formation at both chain ends.

TABLE 1: Enthalpy, Entropy, and Melting Temperature of C35, K35, SG-K35DA, and BK-K35DA

sample	ΔH, kJ mol^{-1}	ΔS, kJ mol^{-1} K^{-1}	T_m, K
SG-C35	135	0.39	347.5
SG-K35	126	0.35	361.6
SG-K35DA	115	0.29	400.7
BK-K35DA	102	0.26	395.6

ends. A small dip is observed at almost the end of the right-hand side of the melting peak for SG-K35DA data. Repeated measurements, however, showed that the position of the dip on the temperature axis as well as its depth varied for every run. At present we have no explanation why this kind of distortion was observed for the SG-K35DA sample.

We calculated enthalpy ΔH and entropy ΔS associated with melting of the four samples from areas of respective endothermic peaks on DSC curves. ΔH and ΔS values of SG- and BK-K35DA listed in Table 1 are smaller than those of C35 and K35. ΔH and ΔS values of SG-K35DA, whose T_m is higher than that of BK-K35DA by about 5 K, are larger than those of BK-K35DA.

Morphologies at Room Temperature. Figure 2shows X-ray diffraction profiles of SG- and BK-K35DA measured at room temperature in a range of diffraction angle 2θ from 1.5° to 30.0°, and also those of SG-C35 and SG-K35 for comparison. SG-C35 gives a sequence of sharp diffraction peaks over a wide diffraction angle range corresponding to (00l) reflections of the long spacing along the main chain c axis with even l as well as two peaks at $2\theta = 21.5°$ and 23.8° from the (110) and (200) planes characteristic of linear alkanes with odd carbon number at room temperature; that is, of the A structure.[15−20] SG-K35 also gives (110) and (200) reflections at the same diffraction angles as SG-C35 and gives sharp peaks corresponding to a sequence of (002l) reflections with odd values of l due to the presence of the carbonyl group in the middle of the molecule.[21−28] On the other hand, BK-K35DA appears to contain a considerable amount of amorphous fraction as evidenced by an amorphous halo in the high diffraction angle region where two diffraction peaks are observed at $2\theta = 21.4°$ and 23.4°, which are very close to those found for SG-C35 with the orthorhombic subcell structure. The amorphous fraction was estimated as 43% from the area of the halo. The profile of SG-K35DA looks a little bit complicated. In addition to peaks found in the same positions as those for BK-K35DA, three new peaks are seen at $2\theta = 5.0°$, 19.0°, and 24.1°. This leads to supposition that SG-K35DA may be polymorphous.

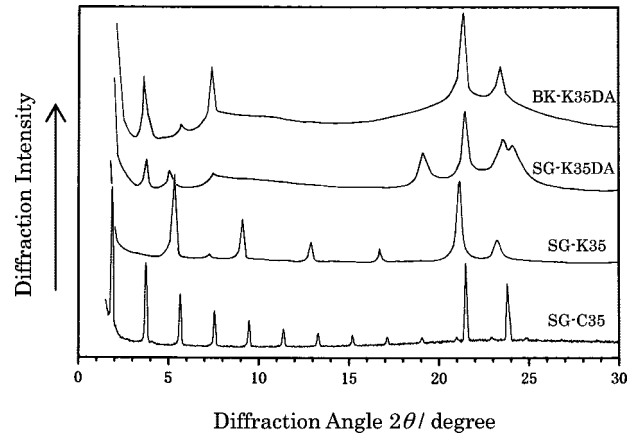

Figure 2. X-ray diffraction profiles for BK-K35DA, SG-K35DA, SG-K35, and SG-C35 at room temperature.

It is well-established from both sides of theory and experiment that two IR absorption bands of linear alkanes, one being the CH_2 rocking mode at 720 cm^{-1} and another the CH_2 scissoring mode at 1473 cm^{-1}, are split into doublets with equal intensity for the orthorhombic subcell structure due to intermolecular interaction, whereas no splitting occurs for other subcell forms. Figure 3 shows results of IR absorption measurements in two regions, 700−750 and 1430−1490 cm^{-1}, at room temperature

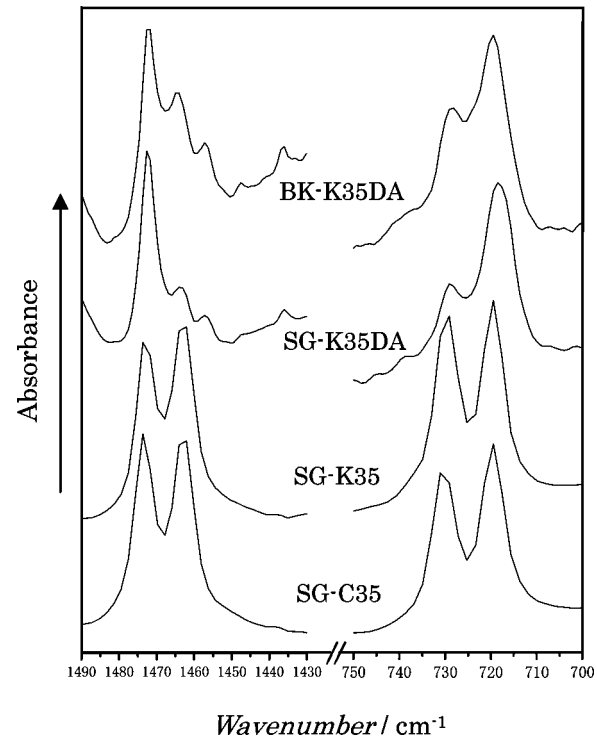

Figure 3. IR spectra for BK-K35DA, SG-K35DA, SG-K35, and SG-C35 in the regions 700−750 and 1430−1490 cm^{-1} at room temperature.

TABLE 2: Comparison of Measured and Calculated Diffraction Angles 2θ for SG- and BK-K35DA

experimental		crystalline lattice calculated			
		$P2_1/c$[a]		$P2_12_12_1$[b]	
2θ, deg	d, nm	2θ, deg	(*hkl*)	2θ, deg	(*hkl*)
		SG-K35DA			
3.5 (m)	2.48			3.6	(004)
5.0 (m)	1.79	5.0	(004)		
7.4 (w)	1.19			7.3	(008)
19.0 (vs)	0.47	19.0	(010)		
21.4 (vs)	0.42			21.4	(110)
23.4 (vs)	0.38			23.4	(200)
24.1 (vw)	0.37	24.1	(200)		
		BK-K35DA			
3.6 (m)	2.47			3.6	(004)
5.5 (vw)	1.61			5.4	(006)
7.4 (m)	1.19			7.3	(008)
21.4 (vs)	0.42			21.4	(110)
23.4 (vs)	0.38			23.4	(200)

[a] $P2_1/c$: $a = 0.958$ nm, $b = 0.466$ nm, $c = 9.34$ nm, $\alpha = \gamma = 90°$, $\beta = 129.8°$, density = 1.17g cm^{-3}. [b] $P2_12_12_1$: $a = 0.759$ nm, $b = 0.497$ nm, $c = 9.52$ nm, $\alpha = \beta = \gamma = 90°$, density = 1.05 g cm^{-3}.

for SG-C35, SG-K35, and SG- and BK-K35DA. The well split IR bands are seen in the spectra of SG-C35 of the A phase and also of SG-K35. Splitting is also clearly observed in the spectra of BK- and SG-K35DA at almost the same wavenumbers as C35 and K35, but there is a considerable difference in doublet intensities. The former result can be considered as additional support for the previous statement that the orthorhombic subcell structure is indeed realized in both SG- and BK-C35DA crystals. Concerning the latter, it can be related to that, for BK-K35DA, there must be a contribution to the spectra from molecules in the amorphous state, which may appear at an intermediate wavenumber between the doublets. The IR contour of BK-K35DA in the region 700−750 cm^{-1} was resolved into crystalline and amorphous components by assuming a Lorentzian profile for each peak by means of a least-squares fitting program.[47] The degree of crystallinity was found to be about 60% from doublet intensities, which is in fair agreement with the corresponding value of 57% calculated from the X-ray diffraction data.

Use of two diffraction peaks at 2$\theta = 21.4°$ and 23.4° for BK-K35DA gives two lattice parameters for the orthorhombic subcell, $a = 0.759$ nm and $b = 0.497$ nm. The remaining task is to determine whether the unit cell is monoclinic or orthorhombic. When the presence of the carbonyl group in the middle and of the carboxyl groups at both ends of the main chain are taken into account, we may assign low-angle diffraction peaks in Figure 2 as (00l) reflections with even l such that peaks of $l = 2$ and 6 become weaker than those of $l = 4$ and 8, and we evaluated the length $c \sin \beta$ as 9.52 nm on average. This value is more than twice the main-chain length of 4.67 nm calculated as the sum of the chain length of C9DA[7] and that of the remaining 26 methylene sequences assumed to take the planar zigzag conformation. Comparison of the two values may lead us to a reasonable conclusion that the unit cell is orthorhombic with $c = 9.52$ nm. It is plausible that neighboring chains randomly translate along the chain axis in order to reduce electrostatic repulsion between the cyclic dimers, which results in an increase of the c value. Results of data analysis are summarized in Table 2.

In addition to the peaks characteristic of the orthorhombic crystal, there remain three diffraction peaks at 2$\theta = 5.0°$, 19.0°, and 24.1°, related to another crystal structure formed in the SG-K35DA sample. It is likely that solution-crystallized K35DA can take a monoclinic-type crystal of either α or β form found for α,ω-alkanedicarboxylic acids with odd n or both. For the α form, in which the main chain is oriented parallel to the c axis, we estimated lattice parameters by setting the lattice parameter c equal to twice the calculated main-chain length; that is, $c = 9.34$ nm. Table 2 lists values of lattice parameters along with assignments to respective peaks. The density calculated is 1.17 g cm^{-3}, which is larger than the corresponding value of 1.05 g cm^{-3} for the coexisting orthorhombic crystal. This indicates that a more densely packed chain arrangement is realized by slow crystallization in dilute solution. We could not reach any clear-cut conclusion whether the β form is present in the SG-K35DA crystal, simply because of a shortage of data points.

We attempted to resolve the methylene rocking band in the region 700−750 cm^{-1} into two components, one being the doublet belonging to the orthorhombic-type crystal and another the singlet belonging to the monoclinic type, by means of the least-squares fitting program used earlier. In spite of the rather forced fit, the right-hand-side peak was found to be decomposed into two peaks with a smaller standard deviation of $\sigma = 0.00034$ compared with the single peak case, and the area corresponding to the monoclinic-type crystal was about 48%.

Structural Changes with Temperature. Changes in the X-ray diffraction profiles of SG- and BK-K35DA with temperature are shown in Figure 4. Both panels clearly indicate that distinct changes occur in the diffraction pattern at elevated temperatures. It is very likely that in temperature region I, below 365 K, SG-K35DA preserves its room-temperature structure and in region III, above 393 K, it is transformed to take the hexagonal structure characterized by one peak at 2$\theta = 21.4°$, together with a new peak at the low diffraction angle of 5.5°. The temperature range of region III looks narrow, followed by melting, and the upper limit is tentatively put as 398 K. In region II, intermediate between I and III, three peaks at 2$\theta = 19.0°$, 23.4°, and 24.1° tend to not only diminish in intensity but also gradually shift toward the central peak at 2$\theta = 21.4°$, which becomes stronger with increasing temperature. The peak at 2$\theta = 5.0°$ is seen to diminish at the same time. These results are very close to the behaviors found in the phase-transition phenomenon of nylon 6/6 by Brill.[35] Transformation of the orthorhombic subcell to a hexagonal one is supported by IR data of the rocking and the scissoring modes. The doublets at room temperature became singlets above 386 K.

Similar phase-transition behavior is also observed for the X-ray diffraction profiles of BK-K35DA: the orthorhombic form in region I transforms to the hexagonal form in region III, which appears to end at 393 K. The peak corresponding to the $(200)_O$ plane starts to decrease in intensity at 378 K; thus the temperature range of region II appears narrower for BK-K35DA than for SG-K35DA. It is to be noted that low diffraction angle peaks are persistently observed above 393 K, while no peak is seen in the high diffraction angle region. This might imply that the hexagonal phase formed in region III could transform to one of the liquid crystalline states before melting with further increase in temperature.

Figure 5 shows temperature-dependent behaviors of the progression bands in the region 1170−1330 cm^{-1} for the two samples. All progression bands are in agreement with each other, not only in wavenumber position but also in relative intensity at room temperature, so that exactly the same assignments may be applicable. Peak intensities of the progression bands in the lower wavenumber region were unexpectedly too low to be used

for discussion. We made assignments by referring to literature in which progression bands of a series of linear alkanes were studied in detail in both experiment and theory.[48,49] We found that excellent agreement was obtained for the progression band data of n-$C_{17}H_{36}$ with 15 methylene units. As shown in the figure, wagging (W) and twisting−rocking (T) modes correspond to the progression bands in this wavenumber region where subscripts express the kth mode given by the expression for the phase angle:

$$\cos \phi_k = k\pi/(n-1) \qquad k = 1, 2, 3, ..., n-2$$

Here n is the carbon number of the n-alkane chain. It is to be noted that relative intensities of the kth wagging modes for odd k are larger than those for even k, which agrees with the finding of Snyder that the wagging mode is active for all k and the intensity for odd k alternates with a less-intensive mode for even k. Unlike n-alkane, a sequence of methylene units is interrupted by introduction of the carbonyl group in the middle of the chain

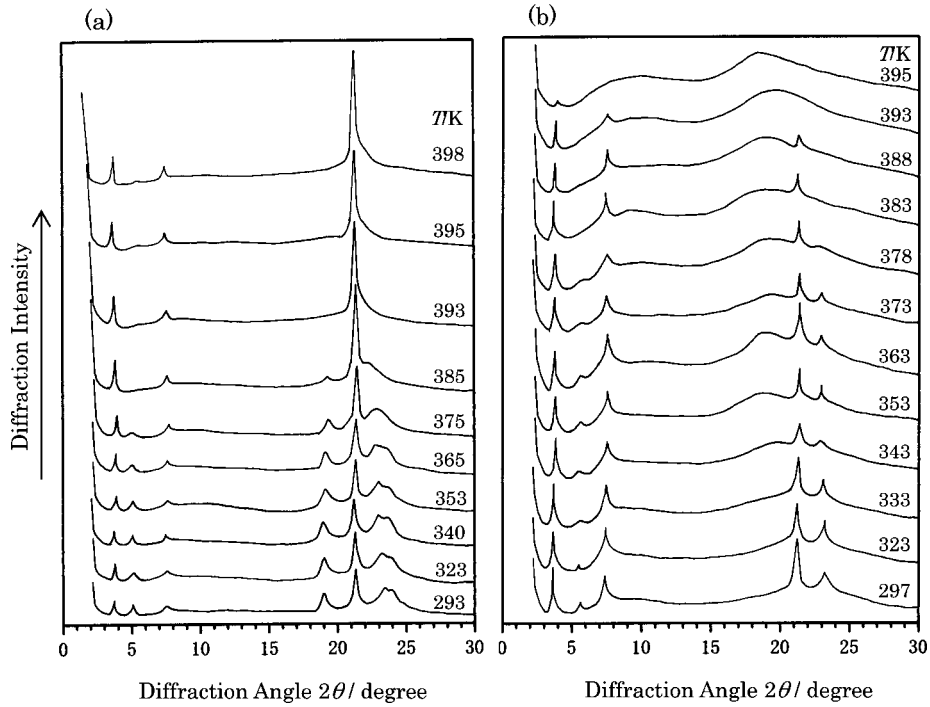

Figure 4. Changes in X-ray diffraction profiles of (a) SG-K35DA and (b) BK-K35DA induced by heat treatment. Measurement temperatures are indicated.

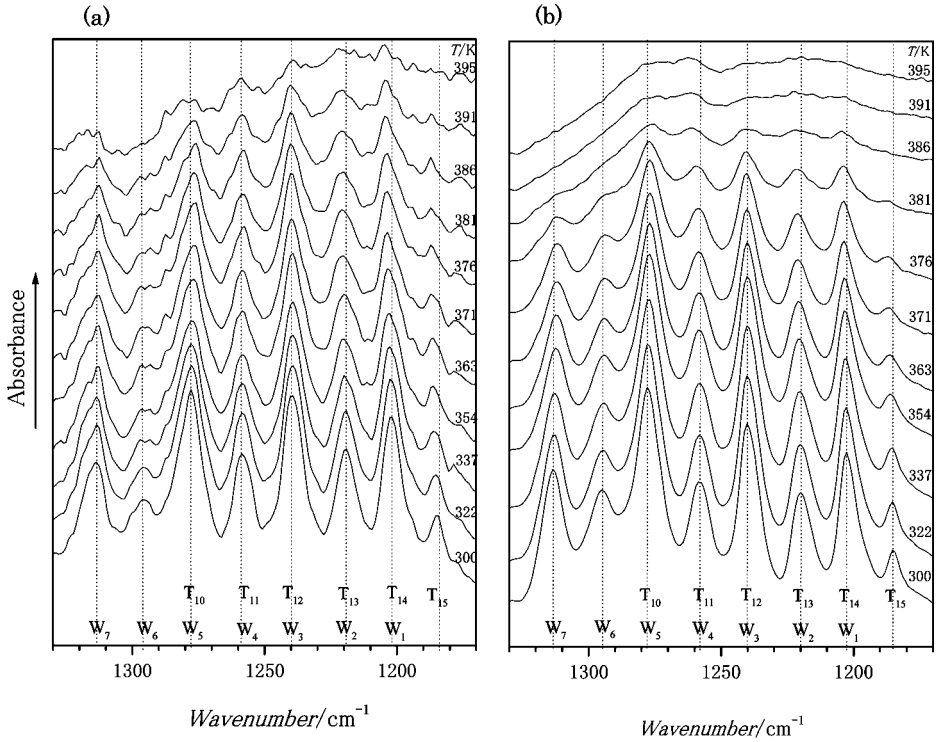

Figure 5. Changes in IR spectra with temperature in the region 1170−1330 cm^{-1} for (a) SG-K35DA and (b) BK-K35DA. Assignments to progression bands are given; W and T denote wagging and twisting−rocking modes, respectively, and subscript k represents their respective kth mode. Measurement temperatures are indicated.

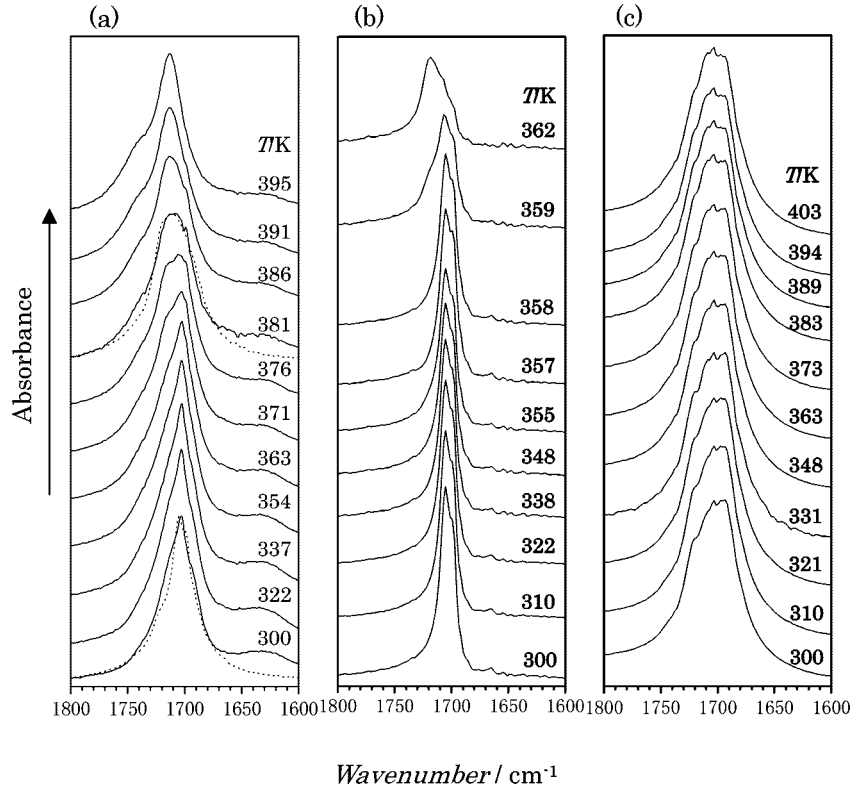

Figure 6. Changes in IR spectra induced by heat treatment in the region 1600−1800 cm^{-1} for (a) SG-K35DA, (b) SG-K35, and (c) SG-C17DA. Measurement temperatures are indicated. Dotted lines at 300 and 381 K in panel a are an attempt to reproduce the IR curves of SG-K35DA by use of data given in panels b and c. Details are given in the text.

for K35DA; thus the number of possible sequential methylene units, m, is considered as 16 from its chemical structure. The difference of one unit between K35DA and n-$C_{17}H_{36}$ may be related to the fact that one chain end is spatially fixed by the cyclic dimer. To examine this simple idea, we measured IR spectra of K35 with free methyl groups at chain ends and the carbonyl group in the middle (thus $m = 16$) as well as C17DA with carboxylic groups at both ends (thus $m = 15$). Progression bands of the former sample were in excellent agreement with those of n-$C_{18}H_{38}$ with $m = 16$, while bands of the latter sample were in good agreement with those of n-$C_{15}H_{32}$ with $m = 13$.[50] These results strongly suggest that spatial fixation of one chain end may affect conformation of neighboring C−C bonds so as to decrease the effective number of methylene units responsible for the progression band by 1. As Figure 5a shows, decreases in intensity are small for all data in region I, where room-temperature crystalline structure is maintained, and above 376 K a substantial decrease appears to start. Such a decrease in intensity indicates that local disordering in chain arrangements is occurring in region II, in harmony with X-ray diffraction data as well as thermal behavior. In region III, where hexagonal chain packing is realized for a short temperature interval, the intensity still decreases and tends to disappear around the melting point identified as the peak minimum of the thermogram.

BK-K35DA behaves in a similar manner as SG-K35DA. Intensities of all modes very gradually decrease with temperature in region I, then rapidly decrease beyond 376 K, and tend to disappear in region III. These results seem to establish that, irrespective of the crystallization method used, solid−solid phase transition of this sample does not take place so sharply as to satisfy the definition of the first-order transition point in equilibrium thermodynamics but gradually proceeds through a temperature interval where chain distortions caused by thermal energy are going to be accumulated.

Useful information on structural changes also may be obtained by studying temperature dependence of the C═O stretching mode, since the carbonyl and carboxyl groups giving this absorption band play an essential role in crystal formation and its stabilization. Figure 6a gives temperature dependence of SG-K35DA IR spectra in the region 1600−1800 cm^{-1}. The band with peak center at 1703 cm^{-1} keeps its shape below 363 K, becomes broader with further increase in temperature, and finally returns to a sharp peak together with a shift of the center to 1713 cm^{-1}. In order to clarify temperature dependences of the carbonyl groups in the middle and at both ends of the K35DA sample separately, we performed IR absorption measurements on SG-K35 and SG-C17DA from room temperature to 395 K, which is above the $T_m = 361.6$ K of SG-K35, and to 403 K, above the $T_m = 392.9$ K of SG-C17DA, respectively. As shown in Figure 6b, the absorption band of 1705 cm^{-1} for SG-K35 exhibits almost no change below 358 K, but at around $T_m = 362$ K the peak rapidly shifts to 1718 cm^{-1}, because dipole directions of the carbonyl residues are randomized as a consequence of melting. The absorption band of C17DA at around 1700 cm^{-1}, composed of a few peaks, does not change from 300 to 403 K beyond its T_m, indicating that hydrogen bonds responsible for the carboxylic dimer are effective over the whole temperature range studied for this sample.

We attempted to reproduce the IR data of SG-K35DA at 300 K belonging to region I and at 381 K to region II using data given in panels b and c. Referring to intensity of the structure-independent C−H stretching band, two data were simply added according to their stoichiometric ratios of C−H bond number. The dotted line at 300 K shows addition of the two data at 300 K, and the line at 381 K indicates addition of the SG-K35 data at 362 K and the SG-C17DA data at 403 K. Reproducibility of experimental curves looks fairly good at 300 K, which confirms that both the hydrogen bonds and the dipole−dipole interaction

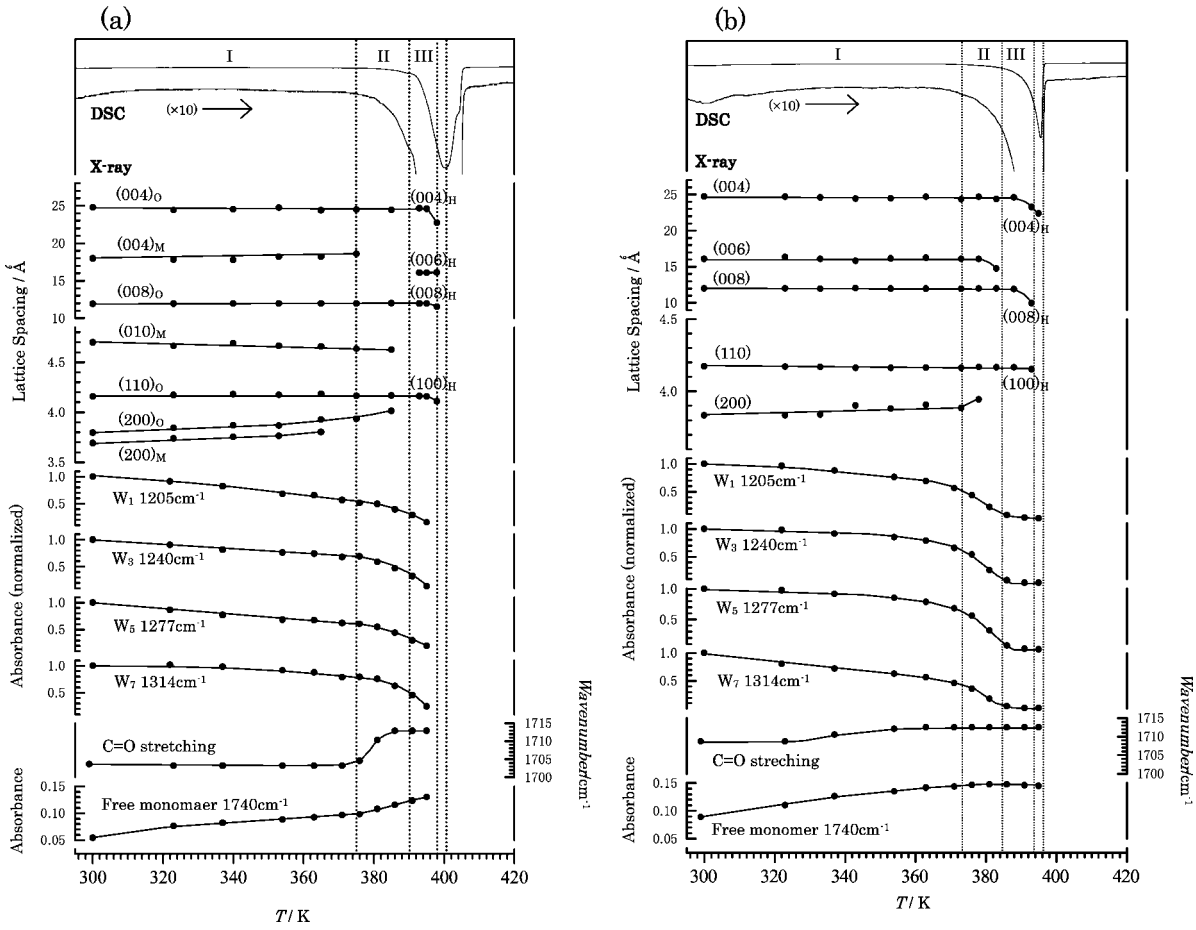

Figure 7. Temperature dependencies of lattice spacings, typical four normalized intensities of the progression bands, and relative intensity and shift of the C═O stretching mode with DSC thermogram. Dotted lines are drawn to show that phase transition behaviors of K35DA can be discussed by dividing into three temperature regions as discussed in detail in the text. (a) SG-K35DA; (b) BK-K35DA. Subscript x in Miller index $(hkl)_x$ in panel a represents that the planes belong to orthorhombic (O), monoclinic (M), or hexagonal (H) types of crystals.

are fully working for maintenance of the crystal structure in region I. On the other hand, a small deviation of the fitted line for 381 K from the experimental data at 1740 cm^{-1} suggests that a few cyclic dimers are broken into free carboxylic monomers in region II, though molecules still may be connected through survived hydrogen bonds. Furthermore, orientation of the carbonyl groups appears to be gradually distorted in region II and to become random at around 381 K. Near the temperature of the phase transition to the hexagonal structure, therefore, molecular motions along the main-chain axis are still severely restricted by hydrogen bonds, whereas molecules are allowed to make thermal motions on the plane vertical to the main-chain axis as if they were in the liquid state. These kinds of differences in temperature dependencies of anisotropic intermolecular forces may rationalize that the Brill transition, classified as the first-order phase transition, is not sharp for this sample as a function of temperature.

Temperature dependence of the broad absorption peak observed for the C═O stretching mode of BK-K35DA is found to be monotonic, which is probably due to contributions from molecules in the amorphous state. Though not shown here, the central peak shifts very gradually with temperature from 1709 to 1713 cm^{-1} and the shoulder at 1740 cm^{-1}, ascribed to a carboxyl monomer free from the hydrogen bond, becomes an independent peak at high temperature. Similar data analysis done for SG-K35DA was not done for BK-K35DA, since we could not obtain IR data for K35DA in the completely amorphous state.

The Brill Transition. The whole aspect of the Brill transition for K35DA is exhibited in Figure 7. In temperature region I, SG-K35DA takes a polymorphic form composed of orthorhombic and monoclinic crystals. Unit cells of the crystals both take the double-layer structure through the carboxylic dimer, so that the strong dipole−dipole interaction brought by carbonyl groups regularly aligned on the plane vertical to the main-chain axis may effectively stabilize the crystal structure. Structural changes accompanied by an endothermic process are clearly observed in region II. First, lattice spacings corresponding to reflections from $(004)_M$, $(010)_M$, and $(200)_M$ planes are going to disappear in this region, and especially the spacing from $(200)_O$ appears to increase rapidly so as to merge into the $(110)_O$ line, which finally becomes only one value characteristic of the hexagonal lattice. Second, distortions of chain alignments inside the crystal are manifested by appreciable decreases in normalized intensities of typical four progression bands in this region. Here normalization is made by use of the corresponding value at 300 K. Third, there occurs a shift of the C═O band from 1703 to 1713 cm^{-1} in region II, which is interpreted as being due to disordering of the carbonyl groups attached in the middle of the main chain. Fourth, intensity at 1740 cm^{-1} is low but monotonously increases with temperature. This corresponds to an increased fraction of free carboxylic monomer, and more various conformational changes along the main-chain direction become possible by breakage of the cyclic dimers. It should be noted that the boundary line at 374 K between regions I and II is drawn to account for these results. After these gradual structural

changes in region II, SG-K35DA transforms to the hexagonal structure characteristic of one lattice spacing corresponding to the $(100)_H$ plane in region III. The phase-transition temperature cannot be located as an independent peak in the DSC curve but appears to be masked by the overwhelming melting process followed. A long period estimated from the $(004)_H$ plane remains constant for a short temperature interval and then decreases with a further increase in temperature. On the other hand, a new reflection corresponding to the $(006)_H$ plane is observed in region III, and its spacing along with that from the $(008)_H$ plane appears to decrease very gradually with increasing temperature. Thus the solid−solid phase transition unambiguously exists for SG-K35DA and the hexagonal phase is maintained at least for several degrees against sufficiently high thermal energy kT where T is close to 400 K.

Figure 7b exhibits results for BK-K35DA. Judging from temperature dependencies of lattice spacings as well as progression bands, it seems reasonable to conclude that BK-K35DA also transforms from orthorhombic crystal through the intervenient temperature region II to the hexagonal one at around 383 K and then melt at 395.6 K, which is lower than $T_m = 400.7$ K of SG-K35DA. Depression of melting point ΔT_m is explained by the fact that BK-K35DA contains a considerable amount of amorphous fraction, 43%. Making use of athermal mixing of crystalline and amorphous components in the liquid state,[51] we calculated $\Delta T_m = 5$ °C, which is in good agreement with the experimental value. A shift of the C═O band is small, and intensity of the free carboxylic monomer starts to increase from room temperature gradually. These may be mainly ascribed to the presence of amorphous components. The lower boundary of region II is determined from the temperature dependence of the progression bands following the procedure adopted for the SG-K35DA case. The temperature 386 K is very close to 385 K for SG-K35DA. It seems that appreciable structural changes are induced by the same level of thermal energy for the two samples. Thus, we may postulate that SG-and BK-K35DA crystals formed under constraints of three different types of intermolecular forces—weak van der Waals interaction, strong hydrogen bonding, and dipole−dipole interaction—exhibit the Brill transition.

Conclusions

We studied solid-state properties of *n*-alkane derivative, K35DA, with a main-chain carbon number $n = 33$ with three functional groups, a carbonyl group in the middle and carboxyl groups at both ends, over a wide temperature range. At room temperature, a crystal with the same orthorhombic subcell structure as long linear alkane was formed independent of the sample preparation method. We showed that at elevated temperature a solid−solid phase transition occurs, whose temperature-dependent behaviors are very close to the Brill transition. As far as we are aware, this sample can be regarded as a new example of the Brill transition, which was hitherto known for nylon *m*/*n* and its model low compounds.

References and Notes

(1) Vanier, P. M.; Brisse, F. *Acta Crystallogr.* **1982**, *B38*, 643.
(2) Gao, Q.; Weber, H.-P.; Ctaven, B. M. *Acta Crystallogr.* **1994**, *B50*, 695.
(3) Housty, P. J. *Bull. Soc. France Miner. Crist.* **1966**, *89*, 307.
(4) Housty, P. J.; Hospital, M. *Acta Crystallogr.* **1965**, *18*, 693.
(5) Housty, P. J.; Hospital, M. *Acta Crystallogr.* **1964**, *17*, 1387.
(6) Housty, P. J.; Hospital, M. *Acta Crystallogr.* **1966**, *20*, 325.
(7) Housty, P. J.; Hospital, M. *Acta Crystallogr.* **1967**, *22*, 289.
(8) Kshunakina, S. I.; Puchkovskaya, G. A. *Zh. Prikl. Spektrosk.* **1981**, *34*, 885.
(9) Housty, P. J.; Hospital, M. *Acta Crystallogr.* **1966**, *21*, 29.
(10) Sintes, P. A.; Housty, P. J.; Hospital, M. *Acta Crystallogr.* **1966**, *21*, 965.
(11) Thalladi, V. R.; Nüsse, M.; Boese, R. *J. Am. Chem. Soc.* **2000**, *122*, 9227.
(12) Boese, R.; Weiss, H. C.; Bläser, D. *Angew. Chem., Int. Ed* **1999**, *38*, 988.
(13) Thalladi, V. R.; Boese, R.; Weiss, H. C. *Angew. Chem., Int. Ed.* **2000**, *39*, 918.
(14) Thalladi, V. R.; Boese, R.; Weiss, H. C. *J. Am. Chem. Soc.* **2000**, *122*, 1186.
(15) Broadhurst, M. G. *J. Res. Natl. Bur. Stand., Sect. A* **1962**, *66*, 241.
(16) Piesczek, W.; Strobl, G. R.; Malzahn, K. *Acta Crystallogr.* **1974**, *B30*, 1278.
(17) Muller, A. *Proc. R. Soc. A* **1932**, *138*, 514.
(18) Bunn, C. W. *Trans. Faraday Soc.* **1939**, *35*, 482.
(19) Mandelkern, L.; Prasad, A.; Alamo, R. G.; Stack, G. M. *Macromolecules* **1990**, *23*, 3696.
(20) Takamizawa, K.; Ogawa, Y.; Oyama, T. *Polym. J.* **1982**, *14*, 441.
(21) Saville, W. B.; Shearer, G. *J. Chem. Soc.* **1925**, *127*, 591.
(22) Muller, A.; Saville, W. B. *J. Chem. Soc.* **1925**, *127*, 599.
(23) Piper, S. H.; Chibnall, A. C.; Hopkins, S. J.; Pollard, A. J.; Smith, A. B.; Williams, B. F. *Biochem. J.* **1931**, *25*, 2072.
(24) Oldham, J. W. H.; Ubbelohde, A. R. *Trans. Faraday. Soc.* **1939**, *35*, 328.
(25) Takamizawa, K.; Nakasone, K.; Urabe, Y. *Colloid Polym. Sci.* **1994**, *272*, 293.
(26) Nakasone, K.; Urabe, Y.; Takamizawa, K. *Thermochim. Acta* **1996**, *286*, 161.
(27) Nakasone, K.; Shiokawa, K.; Urabe, Y.; Nemoto, N. *J. Phys. Chem. B* **2000**, *104*, 7483.
(28) Nakasone, K.; Nemoto, N. *Bull. Chem. Soc. Jpn.* **2007**, *80*, 1316.
(29) Yoshioka, Y.; Tashiro, K.; Ramesh, C. *J. Polym. Sci., Part B: Polym. Phys.* **2003**, *41*, 1294.
(30) Yoshioka, Y.; Tashiro, K. *Polymer* **2003**, *44*, 6407.
(31) Yoshioka, Y.; Tashiro, K. *Polymer* **2003**, *44*, 7007.
(32) Yoshioka, Y.; Tashiro, K. *J. Phys. Chem. B* **2003**, *107*, 11835.
(33) Tashiro, K.; Yoshioka, Y. *Polymer* **2004**, *45*, 4337.
(34) Tashiro, K.; Takeuchi, K.; Ohta, Y.; Hanesaka, M.; Hashida, T.; Yoshioka, Y.; Ramesh, C. *Macromol. Symp.* **2006**, *242*, 250.
(35) Brill, R. *J. Prakt. Chem.* **1942**, *161*, 49.
(36) Itoh, T. *Jpn. J. Appl. Phys* **1976**, *15*, 2295.
(37) Starkweather, H. W.; Jones, G. A. *J. Polym. Sci., Polym., Phys. Ed.* **1981**, *19*, 467.
(38) Kim, K. G.; Newman, B. A.; Scheinbeim, J. I. *J. Polym. Sci., Polym. Phys. Ed.* **1985**, *23*, 2477.
(39) Biangardi, H. J. *J. Macromol. Sci., Phys.* **1990**, *B29*, 139.
(40) Cooper, S. J.; Atkins, E. D. T.; Hill, M. J. *Macromolecules* **1998**, *31*, 8947.
(41) Murthy, N. S.; Wang, Z.; Hisao, B. S. *Macromolecules* **1999**, *32*, 5594.
(42) Jones, N. A.; Atkins, E. D. T.; Hill, M. J. *J. Polym. Sci., Part B: Polym. Phys.* **2000**, *38*, 1209.
(43) Yang, X.; Tan, S.; Li, G.; Zhou, E. *Macromolecules* **2001**, *34*, 5936.
(44) Ramesh, C.; Gowd, E. B. *Macromolecules* **2001**, *34*, 3308.
(45) Ikedo, K.; Yamamoto, Y.; Nagashima, H.; Nemoto, N. *J. Phys. Chem. B* **2005**, *109*, 10668.
(46) Bidd, I.; Whitting, M. C. *J. Chem. Soc., Chem. Commun.* **1985**, *9*, 543.
(47) Cheam, T. C.; Krimm, S. *J. Polym. Sci., Polym. Phys. Ed.* **1981**, *19*, 423.
(48) Snyder, R. G.; Schachtschneider, J. H. *Spectrosc. Acta* **1963**, *19*, 85.
(49) Snyder, R. G. *J. Mol. Spectrosc.* **1960**, *4*, 411.
(50) Yamamoto, H. Ph.D. Dissertation, Kyushu University, 2009.
(51) Yamamoto, H.; Nemoto, N.; Tashiro, K. *J. Phys. Chem.* **2004**, *108*, 5827.

JP808176N